IOP PUBLISHING SEMICONDUCTOR SCIENCE AND TECHNOLOGY

Semicond. Sci. Technol. **26** (2011) 095015 (7pp) doi:10.1088/0268-1242/26/9/095015

Compact drain-current model for reproducing advanced transport models in nanoscale double-gate MOSFETs

M Cheralathan[1], C Sampedro[2], J B Roldán[2], F Gámiz[2], G Iannaccone[3], E Sangiorgi[4] and B Iñiguez[1]

[1] DEEEA, Universitat Rovira i Virgili (URV), Tarragona 43007, Spain
[2] Nanoelectronics Research Group, Department of Electronics, University of Granada, 18071 Granada, Spain
[3] Department of Information Engineering, University of Pisa-IU.NET, Pisa, Italy
[4] ARCES, University of Bologna-IU.NET, Cesena, Italy

E-mail: muthupandian.cheralathan@urv.cat

Received 12 April 2011, in final form 15 June 2011
Published 28 July 2011
Online at stacks.iop.org/SST/26/095015

Abstract
In this paper, we present a double-gate (DG) MOSFET compact model including hydrodynamic transport and quantum mechanical effects in order to extend its application to nanometer technology nodes. The final compact model can accurately reproduce simulation results of some of the most advanced transport simulators. Template devices representative of 22 and 16 nm DG MOSFETs are used. The model is based on a compact model for charge quantization within the channel and it includes mobility degradation, channel length modulation, drain-induced barrier lowering, overshoot velocity effects and quantum mechanical effects. Comparison between the advanced transport modeling approaches and the compact model shows a good degree of agreement within the practical range of voltages.

(Some figures in this article are in colour only in the electronic version)

1. Introduction

Many modeling approaches for the determination of the drain current in MOSFETs are currently used and developed. One of the main reasons behind driving these modeling efforts is the industry need to understand performance improvements due to quasi-ballistic transport and other technology boosters such as strain, high-k dielectrics and extremely thin body silicon-on-insulator (ETSOI) architectures [1]. ETSOI MOS transistors and, in particular, double-gate (DG) MOSFETs are considered to be a very attractive option to improve the performance of CMOS devices. Nanoscale DG-MOSFETs introduce challenges to compact modeling associated with the enhanced coupling between the electrodes (source drain and gates), quantum confinement, ballistic or quasi-ballistic transport, gate tunneling current, etc. For thinner layers, quantum effects start to play a role, but might eventually be considered as a correction to the classical derivation.

In this work, we present the extension of a DG MOSFET model to nanoscale technology nodes by incorporating hydrodynamic transport and quantum mechanical effects, validating it by comparison with numerical 2D transport models ranging from drift-diffusion (DD) to direct solutions of the Boltzmann transport equation (BTE) with the Monte Carlo (MC) method. Our starting point in this work is our previous analytical classical model for the undoped DG MOSFET [2]. We extend this compact model for the drain current to include mobility degradation, short-channel effects (SCE), channel length modulation (CLM), hydrodynamic transport (and therefore velocity overshoot) and quantum effects [3, 4]. The backbone of our model is based on the charge control model [4]. The classical unified charge control model is extended to include quantization effects within the channel using the concept of inversion layer centroid. A correction in the oxide capacitance is included in order to improve the accuracy on the strong inversion region [5]. Finally, we obtain a compact charge control model including quantum effects

 © 2011 IOP Publishing Ltd Printed in the UK & the USA

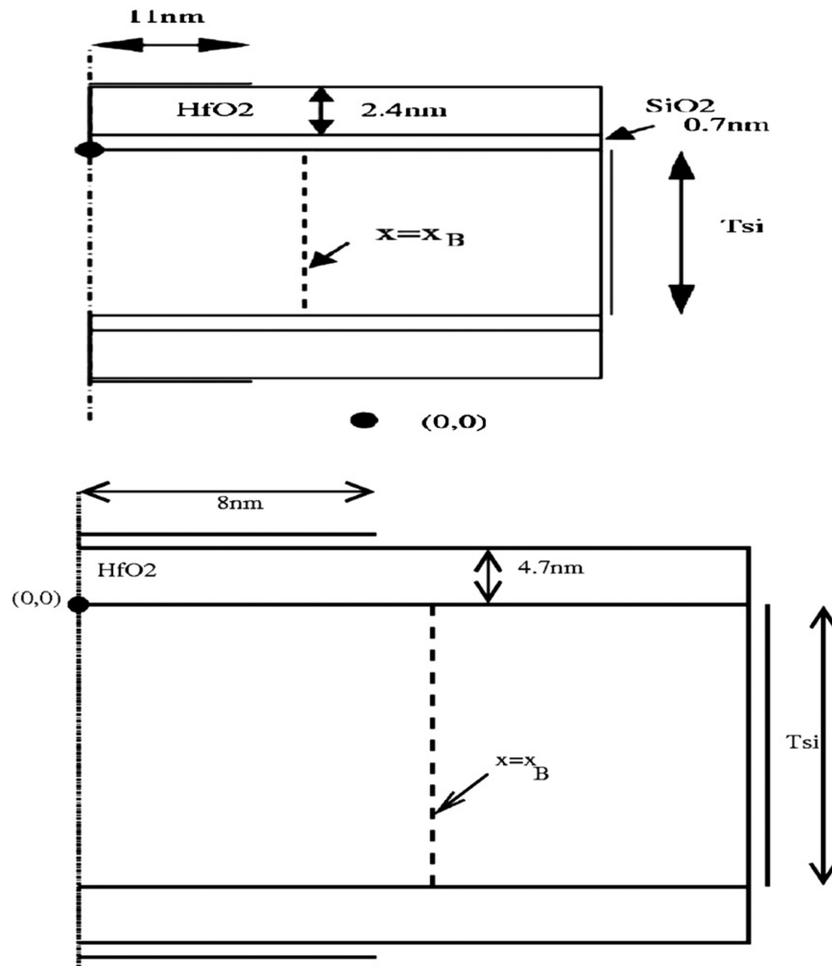

Figure 1. The half structures of the 22 nm (top) and 16 nm (bottom) LSTP DG-MOSFET template used in this work. All the dimensions are in nm.

whose explicit formulation is similar to the classical charge control model. Also, we have included the CLM effect, as well as the role played by quantum effects on the mobility degradation of these devices [6]. The model is validated by comparison with 2D numerical simulations based on different transport models including some of the quantum confinement effects.

2. Simulated devices and approaches

Two different DGSOI transistors have been considered for this study. The first one is an idealized 22 nm channel length device, figure 1 (top), having a gate stack of 2.4 nm of HfO_2 on top of 0.7 nm of SiO_2 (EOT = 1.1 nm) and a silicon film thickness (T_{si}) of 10 nm. The second one is an idealized 16 nm channel length device, figure 1 (bottom), having a gate stack of 4.7 nm of HfO_2 (EOT = 0.8 nm) and a silicon film thickness (T_{si}) of 8 nm. The channels are lowly doped (10^{15} cm^{-3}) in both the devices.

The key features of each model (identified with the acronym of the main developer) are presented. The possible modeling approaches can be grouped in a few families which range from modifications of the conventional DD model used in commercial TCAD tools to advanced MC models. In the DD family, the model gathers DD-like models where only the first momentum of the BTE is calculated. The MC family collects models based on the direct solution of the BTE using the MC method [7]. The MC model incorporates all relevant scattering mechanisms such as ionized impurities (II), surface roughness (SR), phonon scattering, etc. Also, different simulation approaches have been implemented such as full-band, semi-classical and multi-sub-band ensemble MC simulators. The numerical models used by the different groups [8–16] differ in terms of scattering models, simulation approaches, etc. For comparison, all simulators have been first calibrated to reproduce the universal mobility curves as in bulk silicon devices [8].

2.1. DD family

2.1.1. BO-DD. 1D DD solver for SOI-MOSFETs is combined with the solution of the coupled Schrödinger–Poisson equations on the device cross-section normal to the transport direction [10]. The mobility model [11] is also used in the DD solver.

2.2. MC family

2.2.1. BO-MC. The full-band MC simulator treats electrons as a free carrier gas and introduces quantum corrections through the effective potential [12]. Scattering mechanisms include phonons, SR, II in the source/drain.

2.2.2. UD. The multi-sub-band ensemble Monte Carlo (MSMC) simulator is described in [13]. A first-order approach to include quantum effects in the transport direction has been implemented. Scattering mechanisms such as SR and phonons are also included [8].

2.2.3. UPS. The ensemble MC simulator is described in [14]. Quantum corrections are not taken into account here and carriers are treated as a three-dimensional (free) gas in the simulator. All relevant scattering mechanisms are included.

2.2.4. SNPS. The self-consistent semi-classical full-band MC device simulator is described in [15]. Self-consistency is obtained by iterating single-particle simulations with solutions of the nonlinear Poisson equation until convergence. The scattering mechanisms comprise phonon, impurity and SR scattering.

2.2.5. UGR. The MSMC simulator is described in [9]. This method is based on the mode-space approach for quantum transport. All relevant scattering mechanisms are included.

3. DC model

3.1. Classical charge control model

The mobile charge densities at the source Q_s and at the drain Q_d are calculated in [2] and the charge expression also includes the DIBL effect:

$$Q = 2C_g\left(-\frac{2C_g\beta^2}{Q_o\exp\left(\frac{V_{\rm sce}}{\beta}\right)} + \sqrt{\left(\frac{2C_g\beta^2}{Q_o\exp\left(\frac{V_{\rm sce}}{\beta}\right)}\right)^2 + 4\beta^2\log^2\left[1+\exp\left[\frac{V_{gs}-V_{\rm th}+\Delta V_{\rm th}-V}{2\beta}\right]\right]}\right), \quad (1)$$

where $Q_o = 4\beta C_{\rm si}$ and $\beta = \frac{kT}{q}$; $C_{\rm si} = \frac{\varepsilon_{\rm si}}{T_{\rm si}}$ is the silicon-film capacitance, with $\varepsilon_{\rm si}$ the permittivity of silicon and $T_{\rm si}$ the silicon film thickness. $V_{\rm th}$ is defined as

$$V_{\rm th} = V_o + 2\beta\log\left(1+\frac{Q'}{2Q_o}\right), \quad (2)$$

where Q', given in (3), is calculated by solving (1) for Q but using V_o instead of $V_{\rm th}$ (2) and without considering the $\Delta V_{\rm th}$ correction:

$$Q' = C_g\left(-\frac{2C_g\beta^2}{Q_o\exp\left(\frac{V_{\rm sce}}{\beta}\right)} + \sqrt{\left(\frac{2C_g\beta^2}{Q_o\exp\left(\frac{V_{\rm sce}}{\beta}\right)}\right)^2 + 4\beta^2\log^2\left[1+\exp\left[\frac{V_{gs}-V_o-V}{2\beta}\right]\right]}\right), \quad (3)$$

where

$$V_o = \Delta\varphi - \beta\log\left(\frac{qn_iT_{\rm si}}{2Q_o}\right). \quad (4)$$

Here $\Delta\varphi$ is the work-function difference between the gate electrode and the intrinsic silicon and n_i is the intrinsic concentration. In (1), the term $\Delta V_{\rm th}$ ensures the correct behavior of Q above threshold [17],

$$\Delta V_{\rm th} = \frac{\left(\frac{C_g\beta^2}{Q_o}\right)Q'}{Q_o+\frac{Q'}{2}}, \quad (5)$$

where $C_g = \frac{C_{\rm ox}}{\left(1+\frac{C_{\rm ox}y_I}{\varepsilon_{\rm si}}\right)}$ is the effective oxide capacitance, $C_{\rm ox} = \frac{\varepsilon_{\rm ox}}{t_{\rm ox}}$ is the gate-oxide capacitance and $\varepsilon_{\rm ox}$ is the permittivity of oxide.

The inversion centroid is a function of the inversion charge. A simple relationship between the inversion centroid and the inversion charge obtained by fitting numerical simulation results is given by $\frac{1}{y_I} = \frac{1}{a+bT_{\rm si}} + \frac{1}{y_{IO}}\left(\frac{N_I}{N_{IO}}\right)^n$ with $a = 0.35$ nm, $b = 0.26$, $y_{IO} = 6$ nm, $N_{IO} = 7\times10^{12}$ cm^{-2} and $n = 0.8$ [5].

3.2. Velocity overshoot

In an extremely short-channel DG MOSFET, the transport regime is quasi-ballistic; thus, an important overshoot velocity is expected. Using a simplified energy-balance model, the electron mobility is a function of the electron temperature related to the average energy of the carriers. The electron temperature T_e is governed by the following equation [5]:

$$\frac{{\rm d}T_e}{{\rm d}x} + \frac{T_e-T_O}{\lambda_w} = -\frac{q}{2k}E_x(x), \quad (6)$$

where the energy-relaxation length is defined as $\lambda_w \approx 2v_{\rm sat}\tau_w$, with τ_w being the energy relaxation time constant and $v_{\rm sat}$ the saturation velocity, and $E_x(x)$ is the lateral electric field.

The electron velocity in the channel increases as they travel from the source to the drain. However, for a given bias, the velocity can saturate. Assuming this, we can divide the channel into two sections: the first section $0 < x < L_e = L - L_{\rm sat}$ and the saturation region $x > L_e$. In contrast with classical DD models, the saturated velocity in the saturation region due to non-stationary effects can achieve higher values than $v_{\rm sat}$. This phenomenon is known as velocity overshoot [5]. In the linear region, the carrier velocity can be obtained from the mobility as

$$v(x) = \mu_n(x)E_x(x) = \frac{\mu_{\rm eff}}{1+\alpha[T_e(x)-T_O]}E_x(x), \quad (7)$$

where the value of α is determined from (6) under static conditions, where

$$\frac{{\rm d}T_e}{{\rm d}x} = 0: \qquad \alpha = \frac{2k\mu_{\rm eff}}{q\lambda_w v_{\rm sat}}.$$

The energy balance model gives higher currents when compared with the DD model, due to the electron velocity overshoot within the channel. The modified mobility expression given in (7) allows the carrier velocity to exceed the saturation velocity if the channel length becomes comparable with the energy-relaxation length. Thus, the energy relaxation length λ_w inherits the velocity overshoot within its expression.

3.3. Channel length modulation

In order to model the CLM, we need to solve the 2D Poisson's equation in the saturation region [2].

For $V_{ds} < V_{dssat}$, the device works in the linear region. For $V_{ds} > V_{dssat}$, the channel is partially saturated, and the saturated channel length is given by

$$\Delta L = L_c \operatorname{arcsin} h \left(\frac{V_{ds} - V_{dssat}}{E_{sat} L_c} \right), \tag{8}$$

where E_{sat} is the saturation field when velocity reaches saturation.

One of the most used expressions for the saturation potential [18] has been corrected as

$$V_{dssat} = \left(-\frac{Q_{seff}}{2C_g} \right) \left(\frac{v_{sat}}{\left(\frac{-Q_{seff}\mu_{eff}}{4LC_g} \right) + v_{sat}} \right), \tag{9}$$

with

$$Q_{seff} = Q_s + 4\frac{kT}{q} C_g \left(\frac{v_{sat}}{v_{sat} - \frac{kT}{q}\left(\frac{\mu_{eff}}{L}\right)} \right). \tag{10}$$

Thus, Q_{seff} tends to Q_s in strong inversion and to a value that gives the correct V_{dssat} in weak inversion.

A smoothing function is used to interpolate V_{dss}:

$$V_{dss} = V_{ds} - \frac{kT}{q} \frac{\ln\{1 + \exp[A(V_{ds} - V_{dssat})/(kT/q)]\}}{A}, \tag{11}$$

where A is the parameter that controls the transition between saturated and nonsaturated channels.

The saturation characteristic length is given as $L_c = a\sqrt{\frac{\varepsilon_{si} t_{ox} T_{si}}{2\varepsilon_{ox}} + \frac{T_{si}^2}{8}}$. It can be seen that the saturation characteristic length depends only on the device structure and a is a fitting parameter ($0 < a \leqslant 1$).

3.4. DIBL effect

The DIBL effect can be modeled by solving the 2D Poisson's equation in a similar way as for the channel-length modulation [2].

The potential ϕ at the ends of the channel (source and drain) is

$$\phi\,(x = 0) = \phi\,(\phi_c = V_{dss} + V_{bi}) = \phi_d \text{ at the drain}$$

$$\phi\,(x = -L) = \phi\,(\phi_c = 0 + V_{bi}) = \phi_s \text{ at the source,}$$

where V_{bi} is the source and drain junction built-in voltage. The value of the built-in voltage is difficult to calculate in the DG MOSFET because the silicon film is floating. Hence, it can be considered as a fitting parameter:

$$\phi = \phi_c - V_{gs} + V_{fb} - \left(1 + \frac{C_g}{2C_{si}} \left(1 - \frac{1}{n} \right) \right) \left(\left(\frac{Q_s + Q_d}{2} \right) \right) \left(\frac{1}{2C_g} \right), \tag{12}$$

where V_{fb} is the flatband voltage, and Q_s and Q_d are the mobile charges at the source and drain, respectively. If $n = 1$, we have a flat profile, whereas if $n = 2$, we have a parabolic profile. Hence,

$$V_{sce} = 2\sqrt{\phi_s \phi_d} \exp\left(\frac{-L}{2L_c} \right). \tag{13}$$

This quantity, which is equal to zero for long-channel devices [19], can be considered as the barrier potential drop due to the DIBL effect. It is then introduced into the calculation of the charge Q in (1)–(5).

3.5. Drain current

Using the charge control models in (1) and the velocity expression in (7), the expression of the drain current in a DG MOSFET is calculated as a function of the mobile-charge densities at the source Q_s and at the drain Q_d [2]:

$$I_{DS} = \frac{W\mu_{eff}}{L_e(1 + \gamma_n V_{dss})} \left[2\frac{kT}{q}(Q_s - Q_d) + \frac{Q_s^2 - Q_d^2}{4C_g} + 8\left(\frac{kT}{q} \right)^2 C_{si} \log\left[\frac{Q_d + 2Q_o}{Q_s + 2Q_o} \right] \right]. \tag{14}$$

We define the effective mobility as [6]

$$\mu_{eff} = \frac{\mu_o}{1 + \theta_1 \beta \log(1 + \exp(1 + (V_{gs} - V_o)/\beta) + \theta_2 \beta^2 \log(1 + \exp(1 + (V_{gs} - V_o)/\beta)^2}, \tag{15}$$

where μ_o is the low-field mobility, and θ_1 and θ_2 are the mobility attenuation coefficients of the first and second orders, respectively, which can be considered as fitting parameters, $\gamma_n = \frac{\mu_{eff}}{v_{sat} L}\left(\frac{1}{1 + 2\lambda_w/L}\right)$, V_{dss} is equal to V_{ds} for the nonsaturated channel and $V_{dss} = V_{dssat}$ for the saturated channel, and $L_e = L - \Delta L$ and W are the device effective length and width, respectively.

The final compact model for the drain current includes mobility degradation, SCE and CLM. Velocity overshoot is also taken into account through a hydrodynamic transport approach.

3.6. Quantum mechanical effects

Quantum mechanical effects (QME) play a significant role in devices in ultrathin body [20] modifying the electrical behavior in both weak and strong inversion regions. We consider that the first quantum sub-band is mainly responsible for the threshold voltage shift, and the other sub-bands are considered as a geometry dependent correction. The threshold voltage shift is also due to the reduction of oxide capacitance due to the inversion-layer centroid change. In order to accurately model QMEs in all operating regions, we propose an efficient semiempirical approach valid for all ultrathin body given by [21]

$$\Delta E_{qm} = \frac{\hbar^2}{2m_{eff}\beta} \left(\frac{\pi}{T_{si}} \right)^2 \cdot [1 + g(T_{si}, V_{gs})], \tag{16}$$

with

$$g(T_{si}, V_{gs}) = \alpha_{qm1} + \alpha_{qm2} \tfrac{1}{2}\Big[(V_{gs} - V_{fb} - V_o) + \sqrt{(V_{gs} - V_{fb} - V_o)^2}\Big] + \alpha_{qm3} \cdot \tfrac{1}{2}\Big[(V_{gs} - V_{fb} - V_o)^2 + (V_{gs} - V_{fb} - V_o) \cdot \sqrt{(V_{gs} - V_{fb} - V_o)^2}\Big] \tag{17}$$

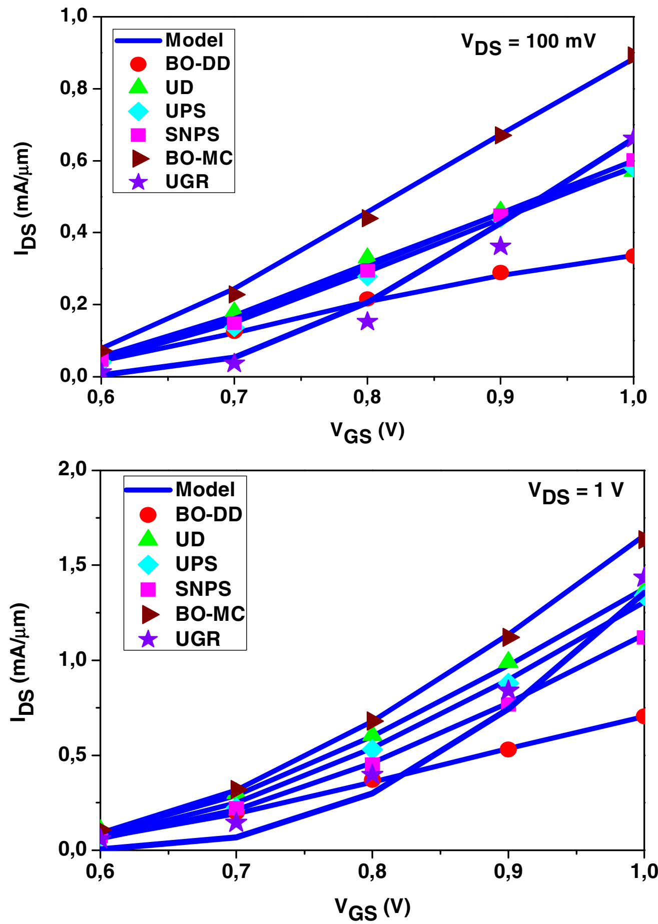

Figure 2. Transfer characteristics of 22 nm DG MOSFETs for low (top) and high (bottom) V_{DS}. 2D numerical simulation data by the University of Bologna (BO-DD) [8], University of Udine (UD) [8], University of Paris-Sud (UPS) [8], Synopsys (SNPS) [8], University of Bologna (BO-MC) [8], University of Granada (UGR) [9].

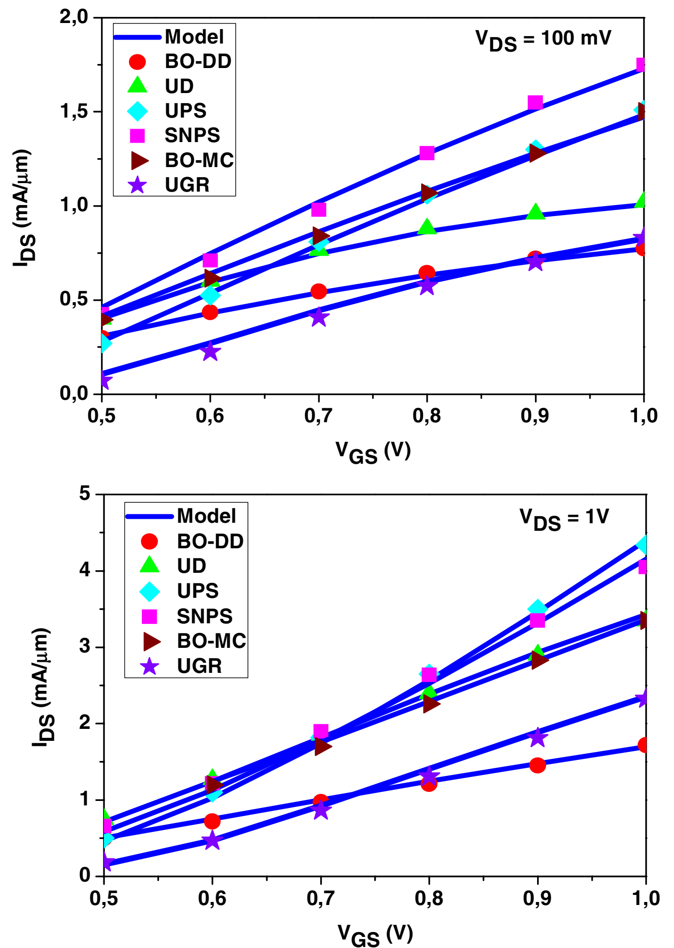

Figure 3. Transfer characteristics of 16 nm DG MOSFETs for low (top) and high (bottom) V_{DS}. 2D numerical simulation data by the University of Bologna (BO-DD) [8], University of Udine (UD) [8], University of Paris-Sud (UPS) [8], Synopsys (SNPS) [8], University of Bologna (BO-MC) [8], University of Granada (UGR) [9].

and

$$\alpha_{qm1} = -0.83 + 0.033 \times T_{si}$$

$$\alpha_{qm2} = -0.011 + 0.0029 \times T_{si} + 0.000\,215 \times T_{si}^2$$

$$\alpha_{qm3} = 0.000\,35 - 0.000\,17 \times T_{si} + 0.000\,046 \times T_{si}^2,$$

where $\hbar$ is the reduced Planck constant, m_{eff} is the electron effective mass and T_{si} is given in nanometers.

Finally, the quantum effects are included in the model as a change in the threshold voltage:

$$V_{O_qm} = V_o + \frac{\Delta E_{qm}}{e}, \quad (18)$$

where e is the electronic charge.

The correction term is added to the V_o term as shown in (18). Thus, the correction makes a positive shift in the threshold voltage of the device (we consider n-channel devices).

4. Results and discussion

The results of the compact model have been compared with the numerical simulation data obtained by several research groups using advanced transport models [7–16]. Figure 2 shows the transfer characteristics of the 22 nm DG MOSFETs at low and high V_{DS}. Good agreement between the compact model and the numerical simulations [8, 9] is obtained by considering the low field mobility and for a fitted saturation velocity. Figure 3 shows the transfer characteristics of the 16 nm DG MOSFETs at low and high V_{DS}. Good agreement is obtained between the compact model and the numerical simulations [8, 9]. In the transfer characteristics, it can be clearly noted that the mobility degradation at low drain voltages is significantly reproduced by the compact model. As expected, the drain-current values provided by the DD model (BO-DD) are lower than those of the other numerical models for both 22 and 16 nm devices.

Figure 4 shows the output characteristics of the 22 and 16 nm DG MOSFETs. Good agreement between the compact model and the numerical simulations [9] is seen. It can be observed that for the model without velocity overshoot and

Table 1. Parameters used in the proposed analytical model in order to fit the simulations obtained using different transport models.

Models	DG MOSFET 22 nm $T_{si} = 10$ nm EOT = 1.1 nm device parameters			DG MOSFET 16 nm $T_{si} = 8$ nm EOT = 0.8 nm device parameters		
	v_{sat} (cm s^{-1})	θ_1 (V^{-1})	θ_2 (V^{-2})	v_{sat} (cm s^{-1})	θ_1 (V^{-1})	θ_2 (V^{-2})
BO-DD	1.1	0.8	1.93	0.9	0.3	1.16
UD	1.02	0.1	0.58	0.92	0.3	1.31
UPS	0.9	0.14	0.039	0.9	0.19	0.19
SNPS	0.9	0.14	0.039	0.8	0.01	0.39
BO-MC	1.01	0.1	0.039	0.8	0.35	0.19
MSB-EMC (UGR)	0.8	0.01	0.05	0.7	0.35	0.9

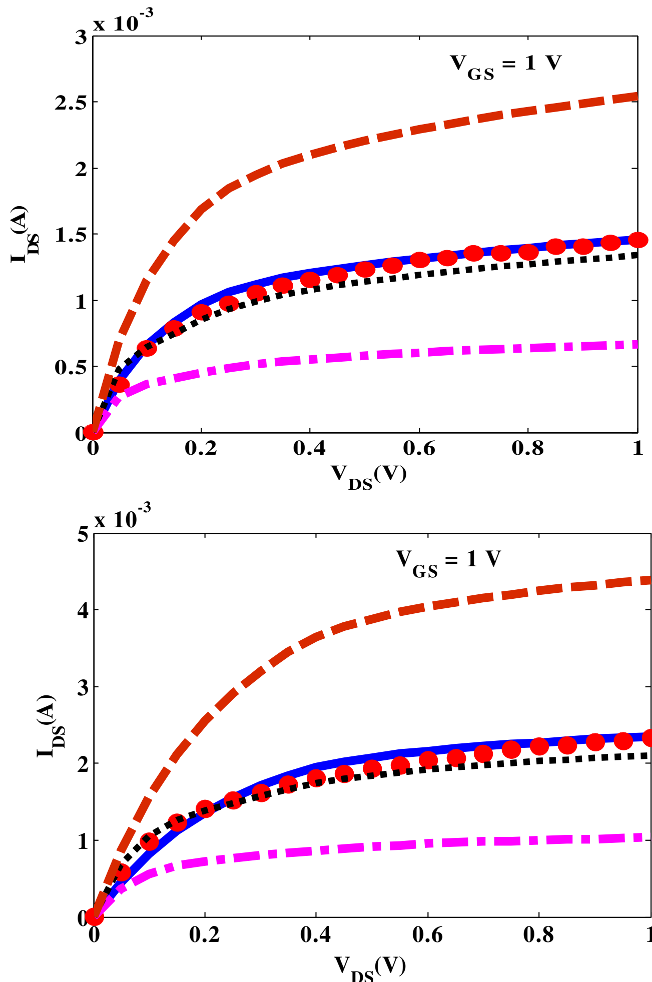

Figure 4. Output characteristics of 22 nm (top) and 16 nm (bottom) DG-MOSFET for $V_{GS} = 1$ V. Dashed line: without quantum effects, solid line: compact model, dotted line: without velocity overshoot and quantum effects, dash-dotted line: without hydrodynamic transport, symbol: simulation (UGR-MSB-EMC) [9].

quantum effects, good agreement is obtained at low drain bias and becomes worse at high drain bias. If the quantum effects are not included in the model, the current becomes significantly higher than the simulations. If the hydrodynamic transport is not considered, the model gives a much lower current than the simulations. Hence, it can be inferred that all these effects should be considered to accurately reproduce results from advanced transport models.

Table 1 indicates the mobility degradation and velocity saturation parameters considered in the model. From the table parameters, it can be seen that strong mobility degradation is observed with the DD model for both devices. It can be seen that low mobility degradation is observed with the UPS simulations for both the devices. The number of fitting parameters used in the compact model is not large (8). The fitting parameters are μ_o, θ_1, θ_2, v_{sat}, a (which controls the characteristic length), V_{fb}, V_{bi} and A (which controls the transition from V_{ds} to V_{dssat}).

5. Conclusion

In this paper, we have extended a compact model for the drain current in DG-MOS transistors. Hydrodynamic transport has been included in a way that can reproduce simulation results of the advanced transport modeling methods. The model is valid and continuous in all operating regimes. Mobility degradation, velocity saturation, short-channel effects and quantum mechanical effects are included. The model shows very good agreement with the 2D simulation results obtained using different transport models for the practical range of voltages considered.

Acknowledgments

This work was supported by the MICINN (Spanish Government) under project TEC2008-06758-C02-02 and TEC2008-06758-C02-01, by the UE under contracts 216171 ‘NANOSIL’, 218255-‘COMON’, EU SQWIRE (FP7-ICT-STREP no 257111) and 216373 ‘EUROSOI+’, by the ICREA Academia Award and by the PGIR grant (URV).

References

[1] International Technology Roadmap for Semiconductor 2009 and the 2010 update, http://public.itrs.net

[2] Lime F, Iñiguez B and Moldovan O 2008 A quasi-two-dimensional compact drain-current model for undoped symmetric double-gate MOSFETs including short-channel effects *IEEE Trans. Electron Devices* **55** 1441–8

[3] Moldovan O, Jiménez D, Guitar J R, Chaves F A and Iñiguez B 2007 Explicit analytical charge and capacitance models of undoped double-gate MOSFETs *IEEE Trans. Electron Devices* **57** 1718–24

[4] Sallese J-M, Krummenacher F, Pregaldiny F, Lallement C, Roy A and Enz C 2004 A design oriented charge-based current model for symmetric DG MOSFET and its correlation with the EKV formalism *Solid-State Electron.* **49** 485–9

[5] Lázaro A, Nae B, Moldovan O and Iñiguez B 2006 A compact quantum model of nanoscale double-gate metal-oxide-semiconductor field-effect transistor for high frequency and noise simulations *J. Appl. Phys.* **100** 084320

[6] Baccarani G and Reggiani S 1999 A compact double-gate MOSFET model comprising quantum-mechanical and nonstatic effects *IEEE Trans. Electron Devices* **46** 1656–66

[7] Palestri P *et al* 2009 Comparison of advanced transport models for nanoscale nMOSFETs *10th Int. Conf. on ULIS 2009* pp 125–8

[8] Palestri P *et al* 2009 A comparison of advanced transport models for the computation of the drain current in nanoscale nMOSFETs *Solid-State Electron.* **53** 1293–302

[9] Sampedro C, Gamiz F, Godoy A, Valin R, Garcia-Loureiro A and Ruiz F G 2010 Multi-subband Monte Carlo study of device orientation effects in ultra-short channel DGSOI *Solid-State Electron.* **54** 131–6

[10] Baccarani G, Gnani E, Gnudi A, Reggiani S and Rudan M 2008 Theoretical foundations of the quantum drift-diffusion and density-gradient models *Solid-State Electron.* **52** 526–32

[11] Reggiani S, Silvestri L, Cacciatori A, Gnani E, Gnudi A and Baccarani G 2007 Physically-based unified compact model for low-field carrier mobility in MOSFETs with different gate stacks and biaxial/uniaxial stress conditions *IEDM Technical. Digest* pp 557–60

[12] Palestri P, Eminente S, Esseni D, Fiegna C, Sangiorgi E and Selmi L 2005 An improved semi-classical Monte-Carlo approach for nano-scale MOSFET simulation *Solid-State Electron.* **49** 727–32

[13] Lucci L, Palestri P, Esseni D, Bergagnini L and Selmi L 2007 Multi-subband Monte-Carlo study of transport, quantization and electron gas degeneration in ultra-thin SOI n-MOSFETs *IEEE Trans. Electron Devices* **54** 1156–64

[14] Querlioz D, Saint-Martin J, Huet K, Bournel A, Aubry-Fortuna V, Chassat C, Galdin-Retailleau S and Dollfus P 2007 On the ability of the particle Monte Carlo technique to include quantum effects in nano-MOSFET simulation *IEEE Trans. Electron Devices* **54** 2232–42

[15] Bufler F M, Asahi Y, Yoshimura H, Zechner C, Schenk A and Fichtner W 2003 Monte Carlo simulation and measurement of nanoscale n-MOSFETs *IEEE Trans. Electron Devices* **50** 418–24

[16] Bufler F M *et al* 2010 Comparison of semiclassical transport formulations including quantum corrections for advanced devices with high-K gate stacks *Proc. 14th IWCE 2010 (Pisa, Italy)* pp 319–22

[17] Iñiguez B, Jiménez D, Roig J, Hamid H A, Marsal L F and Pallares J 2005 Explicit continuous model for long-channel undoped surrounding gate MOSFETs *IEEE Trans. Electron Devices* **52** 1868–73

[18] Iñiguez B and Garcia-Moreno E 1997 An improved C_∞-continuous small-geometry MOSFET modeling for analog applications *Analog Integr. Circuits Signal Process.* **13** 241–59

[19] Yan R H, Ourmazd A and Lee K F 1992 Scaling the Si MOSFET: from bulk to SOI to bulk *IEEE Trans. Electron Devices* **39** 1704–10

[20] Gamiz F and Fischetti M 2001 Monte Carlo simulation of double-gate silicon-on-insulator inversion layers: the role of volume inversion *J. Appl. Phys.* **89** 5478

[21] Tang M, Pregaldiny F, Lallement C and Sallese J-M 2009 Explicit compact model for ultranarrow body FinFETs *IEEE Trans. Electron Devices* **56** 1543–7